

THE EFFECT OF ACTINIDES ON THE MICROSTRUCTURAL DEVELOPMENT IN  
A METALLIC HIGH-LEVEL NUCLEAR WASTE FORM<sup>1</sup>

by

RECEIVED  
JAN 18 2000  
OSTI

Dennis D. Keiser, Jr.<sup>a</sup>, Wharton Sinkler<sup>a</sup>, Daniel P. Abraham<sup>b</sup>, James W. Richardson, Jr.<sup>b</sup>,  
and Sean M. McDevitt<sup>b</sup>

<sup>a</sup>Argonne National Laboratory-West, P. O. Box 2528, Idaho Falls, ID 83403-2528

<sup>b</sup>Argonne National Laboratory, 9700 S. Cass Ave., Argonne, IL 60439-4803

The submitted manuscript has been created by the University of Chicago as Operator of Argonne National Laboratory ("Argonne") under Contract No. W-31-109-ENG-38 with the U.S. Department of Energy. The U.S. Government retains for itself, and others acting in its behalf, a paid-up, nonexclusive, irrevocable worldwide license in said article to reproduce, prepare derivative works, distribute copies to the public, and perform publicly and display publicly, by or on behalf of the Government.

Paper to be Published in *Rare Earths and Actinides: Science, Technology and Applications IV* and to be Presented at the TMS Annual Meeting, Nashville, TN, March 12-16, 2000.

---

<sup>1</sup> Work supported by the U.S. Department of Energy, Office of Nuclear Energy, Science, and Technology, under contract W-31-109-Eng-38.

## DISCLAIMER

This report was prepared as an account of work sponsored by an agency of the United States Government. Neither the United States Government nor any agency thereof, nor any of their employees, make any warranty, express or implied, or assumes any legal liability or responsibility for the accuracy, completeness, or usefulness of any information, apparatus, product, or process disclosed, or represents that its use would not infringe privately owned rights. Reference herein to any specific commercial product, process, or service by trade name, trademark, manufacturer, or otherwise does not necessarily constitute or imply its endorsement, recommendation, or favoring by the United States Government or any agency thereof. The views and opinions of authors expressed herein do not necessarily state or reflect those of the United States Government or any agency thereof.

## **DISCLAIMER**

**Portions of this document may be illegible in electronic image products. Images are produced from the best available original document.**

# THE EFFECT OF ACTINIDES ON THE MICROSTRUCTURAL DEVELOPMENT IN A METALLIC HIGH-LEVEL NUCLEAR WASTE FORM

Dennis D. Keiser, Jr.<sup>a</sup>, Wharton Sinkler<sup>a</sup>, Daniel P. Abraham<sup>b</sup>, James W. Richardson, Jr.<sup>b</sup>, and Sean M. McDevitt<sup>b</sup>

<sup>a</sup>Argonne National Laboratory-West, P. O. Box 2528, Idaho Falls, ID 83403-2528

<sup>b</sup>Argonne National Laboratory, 9700 S. Cass Ave., Argonne, IL 60439-4803

## Abstract

Waste forms to contain material residual from an electrometallurgical treatment of spent nuclear fuel have been developed by Argonne National Laboratory. One of these waste forms contains waste stainless steel (SS), fission products that are noble to the process (e.g., Tc, Ru, Pd, Rh), Zr, and actinides. The baseline composition of this metallic waste form is SS-15wt.% Zr. The metallurgy of this baseline alloy has been well characterized. On the other hand, the effects of actinides on the alloy microstructure are not well understood. As a result, SS-Zr alloys with added U, Pu, and/or Np have been cast and then characterized, using scanning electron microscopy, transmission electron microscopy, and neutron diffraction, to investigate the microstructural development in SS-Zr alloys that contain actinides. Actinides were found to congregate non-uniformly in a  $Zr(Fe,Cr,Ni)_{2+x}$  phase. Apparently, the actinides were contained in varying amounts in the different polytypes (C14, C15, and C36) of the  $Zr(Fe,Cr,Ni)_{2+x}$  phase. Heat treatment of an actinide-containing SS-15 wt.% Zr alloy showed the observed microstructure to be stable.

## Introduction

A variety of waste forms have been developed for possible use in disposing of actinides in a geologic repository [1]. Some of these waste forms include glass, SYNROC, and actual spent nuclear fuel. Another waste form that contains actinides is being developed by Argonne National Laboratory. It is a metallic waste form, and it contains material residual from an electrometallurgical treatment that is used to extract usable uranium from spent nuclear fuel [2]. Some of this residual material is comprised of actinides. This metallic waste form (MWF) is a stainless steel-Zr alloy, and in addition to actinides (U, Pu, Np) it contains stainless steel cladding, "noble" metal fission products (Pd, Ru, Tc, etc.)<sup>1</sup> and zirconium, which is an element of the alloy fuel being treated. The baseline waste form composition is stainless steel (SS)- 15 wt.% Zr. Early tests have shown that this baseline alloy is durable and corrosion-resistant and would make a good waste form in comparison to other waste forms [3].

One important factor in guaranteeing that the MWF will perform adequately in a geologic repository is by having a good understanding of how the presence of actinides affects microstructural development in the alloy and of how these elements partition between alloy phases. To obtain such an understanding, a variety of MWF alloys have been generated with different actinide concentrations. These alloys have then been characterized using scanning electron microscopy, neutron diffraction, and transmission electron microscopy. The influence of having the actinides present in the alloy has been determined by comparing the characterization results for these alloys with those generated for SS-15Zr<sup>2</sup> alloys without actinides. One alloy was heat treated to confirm the stability of the observed microstructure. Results of corrosion tests on actinide-containing SS-Zr alloys will be reported in future articles.

## Background

The baseline SS-15Zr alloy is observed to have a eutectic microstructure that is comprised of two major phases [4]. These phases include an Fe solid solution phase, primarily ferrite, and an  $Zr(Fe,Cr,Ni)_{2+x}$  intermetallic phase that is substoichiometric in Zr. Some minor phases have also been observed, viz. austenite and  $Fe_{23}Zr_6$ . Since the  $Zr(Fe,Cr,Ni)_{2+x}$  intermetallic phase is a Laves phase ( $AB_2$ ), different polytypes of this phase could possibly be present in a SS-15Zr alloy. Possible polytypes are C14 (hexagonal;  $MgZn_2$ -type), C15 (cubic;  $MgCu_2$ -type), and C36 (dihexagonal;  $MgZn_2$ -type). Neutron diffraction results have shown that C15 and C36 are the primary polytypes of the  $Zr(Fe,Cr,Ni)_{2+x}$  intermetallic phase that are present in a SS-15Zr alloy [5].

## Experimental Procedure

To investigate the effects of adding actinides to a 316SS-15Zr alloy, ten actinide-containing 316SS-15Zr alloys were cast in one of two ways. Six were cast using an induction furnace, and the others were generated using a resistance furnace. The induction furnace-generated alloys were cast, as approximately 30 gram charges, in yttrium oxide ceramic crucibles (65 mm tall, 43 mm o.d., and 3 mm wall thickness). The alloy compositions included: 316SS<sup>3</sup>-15Zr-0.5U-0.5Pu, 316SS-15Zr-2U-2Pu, 316SS-15Zr-2Np, 316SS-15Zr-6Pu-2Np, 316SS-15Zr-6Pu, and 316SS-15Zr-10Pu. The melting and solidification procedure involved heating the charged crucibles to 1600°C under flowing argon, holding for 2 hours, then cooling the ingots down to 1500°C, 1400°C, 1300°C, and 1200°C, and holding for 15 minutes at each of these temperatures. At 1200°C, the furnace was turned off. The cooling sequence lessened the chance for cracking the yttria crucibles, which have low thermal shock resistance.

The alloys cast using a resistance furnace employed 10 grams of charge. The alloy compositions included: 316SS-15Zr-5U, 316SS-15Zr-1Nb-1Ru-1Rh-1Pd-1Tc-2U, 316SS-15Zr-0.6Ru-0.3Tc-0.1Pd-11U, and 316SS-15Zr-2Tc-5U. The Nb, Ru, Rh, Pd, and Tc were

<sup>1</sup> These are elements that are noble to the electrometallurgical treatment process.

<sup>2</sup> Alloy compositions are listed in wt.%.

<sup>3</sup> Type 316 stainless steel has the following nominal composition (in wt.%): 10-14Ni-16-18Cr-2Mn-2-3Mo-1Si-0.08C-0.03S-0.045P-bal.Fe.

added as surrogates for the "noble" metal fission products. The casting procedure consisted of placing the alloy charge in yttrium oxide crucibles (17mm dia. and 49 mm tall), heating them to 1600°C under an argon atmosphere, holding them at temperature for approximately 1 hour, and then cooling them slowly (<10°C/min.) to room temperature.

Microstructural characterization was performed on samples sliced, using a diamond saw, from the as-cast buttons and polished through 1- $\mu$ m diamond paste. Using both a Zeiss DSM960A and an ETEC Autoscan scanning electron microscope (SEM), both operated in secondary and backscattered electron modes, the samples were characterized. For composition information, the Zeiss 960A SEM was equipped with an Oxford energy dispersive spectrometer (EDS) and wavelength dispersive spectrometer (WDS) along with LINK\_ISIS software. The ETEC Autoscan SEM was equipped with a Kevex 8000 (Fisons Instruments) EDS system.

Additional microstructural analysis was performed on a sample taken from the 316SS-15Zr-2Tc-5U alloy using a JEOL 2010 transmission electron microscope (TEM) operated at 200kV, TEM foils were produced by slicing using a diamond saw. The slices were reduced by grinding to a thickness of approximately 250  $\mu$ m using 400 grit SiC paper. Following this, 3 mm disks were cut from the thin section, and further thinned mechanically using lapping papers to a final thickness of between 60  $\mu$ m and 100  $\mu$ m. The polished disks were dimpled to a central thickness of approximately 15  $\mu$ m, and then ion milled to perforation using a Gatan PIPS ion mill.

The as-cast 316SS-15Zr-5U alloy was analyzed using neutron diffraction to definitively identify the phases present in actinide-containing SS-15Zr-based alloys. Time-of-flight (TOF) neutron diffraction data were collected on the General Purpose Powder Diffractometer at the Intense Pulsed Neutron Source (IPNS). TOF experiments are carried out at a fixed scattering angle, and diffraction patterns are generated as a function of incident neutron wavelength. Diffraction data are obtained at six separate detector banks, each positioned at a fixed angle relative to the incident beam. Since each detector bank views the sample from a different orientation, an assessment of preferred orientation (texture) in the sample can be obtained from variations in intensity from bank to bank. Reitveld refinements were carried out on the neutron diffraction data to obtain the lattice parameters and volume content of phases observed in the sample.

The 316SS-15Zr-10Pu alloy was given a homogenizing heat treatment to investigate the stability of the observed microstructure. The sample was placed in a yttria crucible and sealed within an Inconel-600 annealing capsule. The capsule was evacuated and back-filled several times with high-purity argon prior to the annealing, which was performed at 851°C  $\pm$  4°C for 100 hours.

## Results

### Microstructural Characterization

SEM Analyses. The microstructure of a 316SS-15Zr-5U alloy is presented in Figure 1. This microstructure is representative of the ones observed for all SS-15Zr alloys with added actinides. Two major phases comprise the microstructure shown in Figure 1: an Fe solid solution phase, mainly ferrite, and a Zr(Fe,Cr,Ni)<sub>2+x</sub> phase. Within the Zr(Fe,Cr,Ni)<sub>2+x</sub> phase are located actinide-rich regions that exhibit bright contrast in an SEM micrograph (see Figure 1). Actinides were observed only within the Laves intermetallic. The bright areas seen in Fig. 1, have a larger proportion of actinides than the rest of the Laves intermetallic. The actinide content showed a gradual

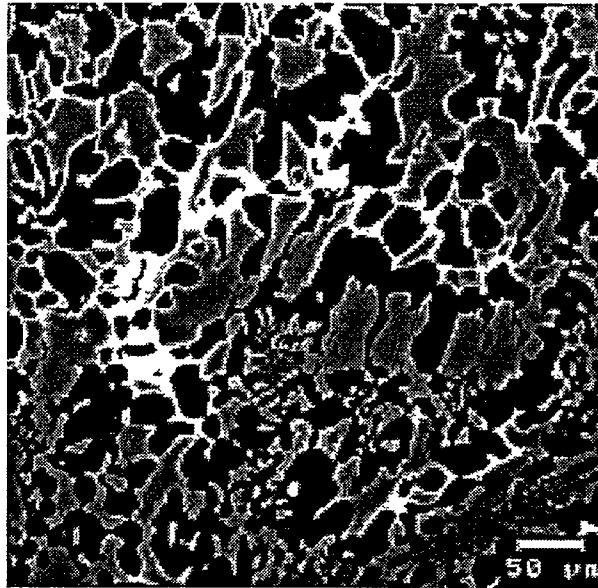


Figure 1. Typical microstructure observed in a SS-15Zr-5U alloy. The bright areas are uranium-rich regions within the Laves intermetallic (gray phase). The dark phase is ferrite. This microstructure is representative of what is observed in all actinide-containing alloys.

decrease between the bright areas and adjoining areas in the Laves intermetallic; distinct interphase boundaries were not observed. The compositions of the major phases observed in the 316SS-15Zr-5U alloy are listed in Table I. It was observed

Table I. Composition of Phases Observed in the 316SS-15Zr-5U Alloy.

Phases	Composition (At.%)							
	Fe	Cr	Ni	Zr	Mn	Mo	Si	U
Ferrite	67.5	23.2	5.0	Neg.	2.6	1.1	0.8	Neg.
U-rich $Zr(Fe,Cr,Ni)_{2+x}$	44.9	3.3	25.7	7.6	1.4	Neg.	0.3	17.2
$Zr(Fe,Cr,Ni)_{2+x}$	49.1	6.0	18.0	20.6	2.5	0.9	1.5	1.5

that for most of the actinide-containing SS-15Zr alloys the sum of the actinides and Zr concentrations in the  $Zr(Fe,Cr,Ni)_{2+x}$  phase was close to 24 at.%. The exception was observed for the Np-containing alloys where the sum of the actinide and Zr concentrations was nearer to 14 at.%. As more actinides were added to the SS-15Zr alloy, more of the actinide-rich regions were observed. Minor phases are typically observed in SS-15Zr alloys [5]. These phases include austenite and an  $Fe_{23}Zr_6$  intermetallic, but they were not observed in the sample taken from the 316SS-15Zr-5U alloy and analyzed using the SEM. Yet, in some of the other alloys that were cast, the minor phase  $Fe_{23}Zr_6$  was observed using the SEM (e.g., the 316SS-15Zr-11U-0.6Ru-0.3Tc-0.1Pd alloy). Austenite was not successfully resolved in the actinide-containing SS-15Zr alloys using the SEM.

The microstructure of the 316SS-15Zr-10Pu alloy that was heat-treated at 851°C for 100 hours is presented in Figure 2. No changes in the alloy microstructure were observed after heat treatment. The phase compositions were analogous before and after heat treatment.

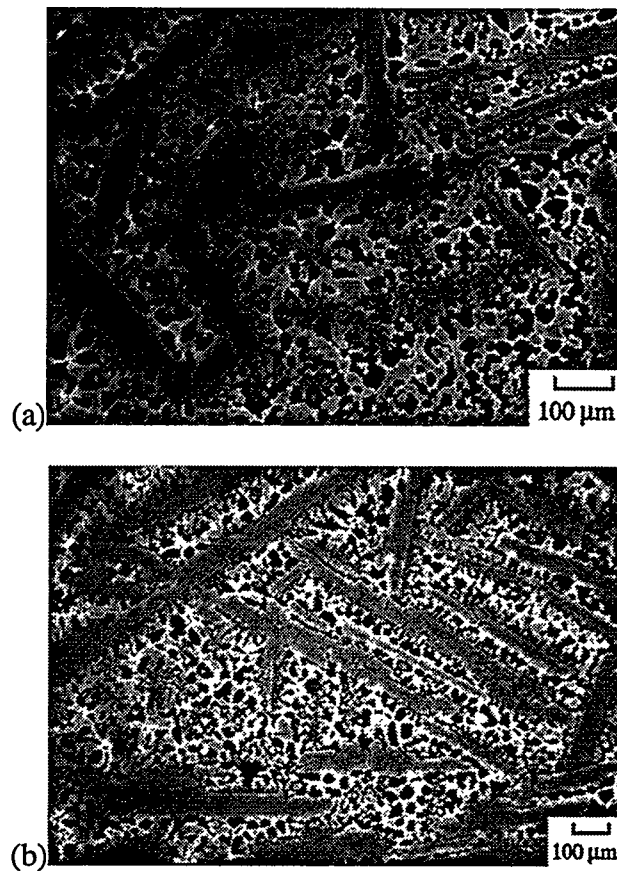


Figure 2. Backscattered electron micrographs of (a) an as-cast 316SS-15Zr-10Pu alloy and (b) a 316SS-15Zr-10Pu alloy heat-treated at 851°C for 100 hours.

**TEM Analyses.** Figure 3 a-d shows portions of several X-ray-EDS spectra taken from different areas of the TEM samples produced from the 316SS-15Zr-5U-2Tc alloy, and Fig. 4 a-d shows the corresponding selected area diffraction patterns (SADP's) from the four Laves phase polytypes that were observed. These are the standard 2 and 4 layer hexagonal structures (*Strukturbericht* designations C14 and C36), as well as the 3-layer cubic (C15) and a 6-layer hexagonal structure, found in previous work on the Ti-Co system [6]. The spectra in Figure 3 show primarily the U-L $\alpha$  and Zr K $\alpha$ 1 characteristic lines at 13.615 keV and 15.747 keV respectively. As can be seen, there is a pronounced variation of the relative peak intensities for these peaks, for the different structures indicated in Figure 4, with the cubic C15 structure consistently having a larger relative intensity of the U-L $\alpha$  line, than the other hexagonal polytypes. According to the Cliff-Lorimer ratio technique, the relative concentrations of U and Zr are given by [7]:

$$\frac{x_U}{x_{Zr}} = k_{U,Zr} \frac{I_U}{I_{Zr}}$$

where  $I_U$  and  $I_{Zr}$  are the integrated intensities of a characteristic X-EDS lines of U and Zr, respectively, and  $k_{U,Zr}$  is the Cliff-Lorimer factor, which may be obtained using a standard. Table II shows a number of measurements of  $I_U/I_{Zr}$  from several areas in which the polytype could be positively identified using selected area diffraction. No standard was available to determine the value of  $k_{U,Zr}$ , and the actual relative concentrations are thus not known. It may, however, reasonably be assumed that the range of values of  $I_U/I_{Zr}$  correspond roughly to the concentration ranges found using SEM. While absolute concentrations are not available from the present data, it is nevertheless clear from Table II that the C15 phase consistently contained the most U, while C14 contains the least, and C36 as well as the six-layer hexagonal polytype (6H) had intermediate uranium concentrations. This is consistent with a uranium concentration

which scales with the cubic character of the compound involved (see e.g. [8]). In the present study, the area richest in uranium (position 1 in Table II) was immediately adjacent to a region of ferrite phase. This is consistent with SEM investigation of this sample, in which uranium tended to segregate to the edges of Laves compound regions.

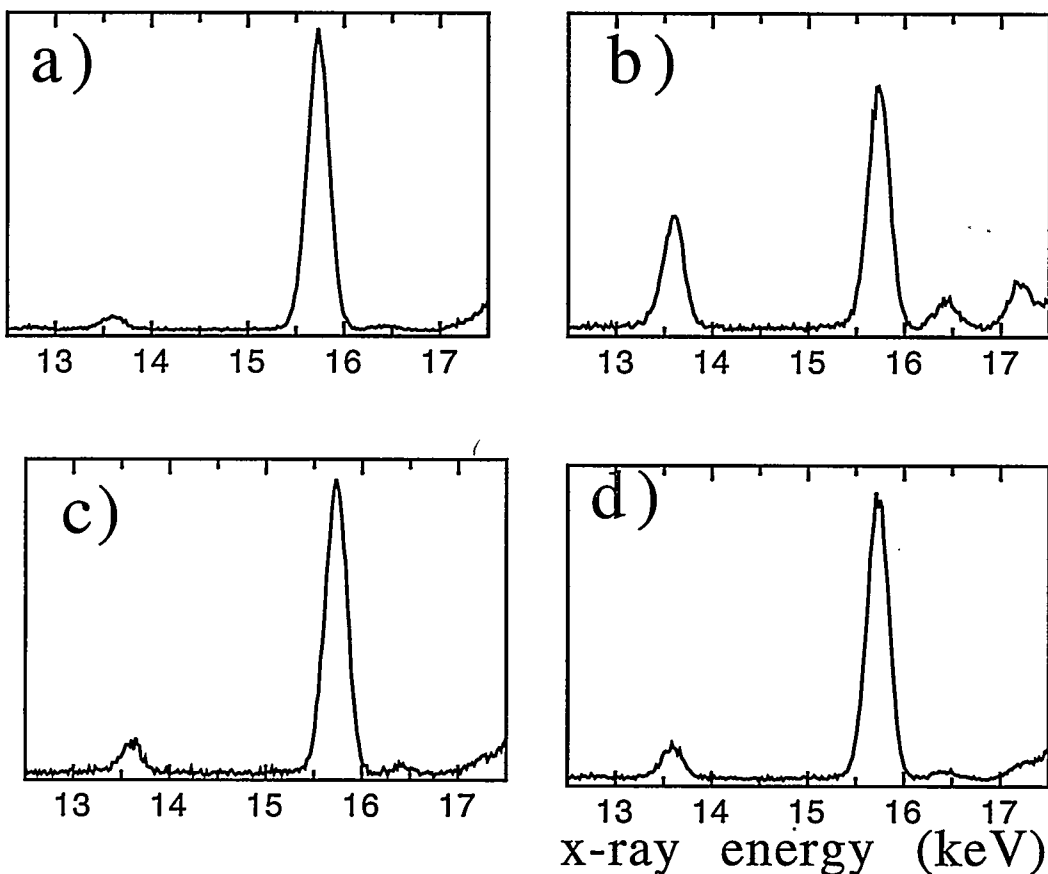


Figure 3. Portions of TEM X-ray-EDS spectra for various positions in sample, showing the U-L $\alpha$ 1 and Zr-K $\alpha$ 1 characteristic lines. The crystal structures were fingerprinted using transmission electron diffraction, and are a) C14, b) C15, c) C36 and d) 6H.

Neutron Diffraction Analyses. The neutron diffraction pattern obtained from the SS-15Zr-5U alloy is shown in Figure 5. Peaks corresponding to five phases were identified: ferrite, austenite, ZrFe<sub>2</sub>-type Laves polytypes C36 and C15 and a Fe<sub>23</sub>Zr<sub>6</sub>-type intermetallic. These phases are the same as those observed in a SS-15Zr alloy without uranium [5]. Peaks corresponding to U-rich phases were not observed in the neutron diffraction patterns. Minor uranium oxide peaks observed in the diffraction patterns were from the melt-crucible interaction residue on the alloy specimens, and have not been included in our analyses. The lattice parameters and volume content of the phases are listed in Table III. The influence of texture on phase content was minimized by averaging the results from all detector banks. These neutron diffraction results proved especially useful since the austenite and the Fe<sub>23</sub>Zr<sub>6</sub>-type intermetallic could not be identified in the 316SS-15Zr-5U alloy using the SEM.

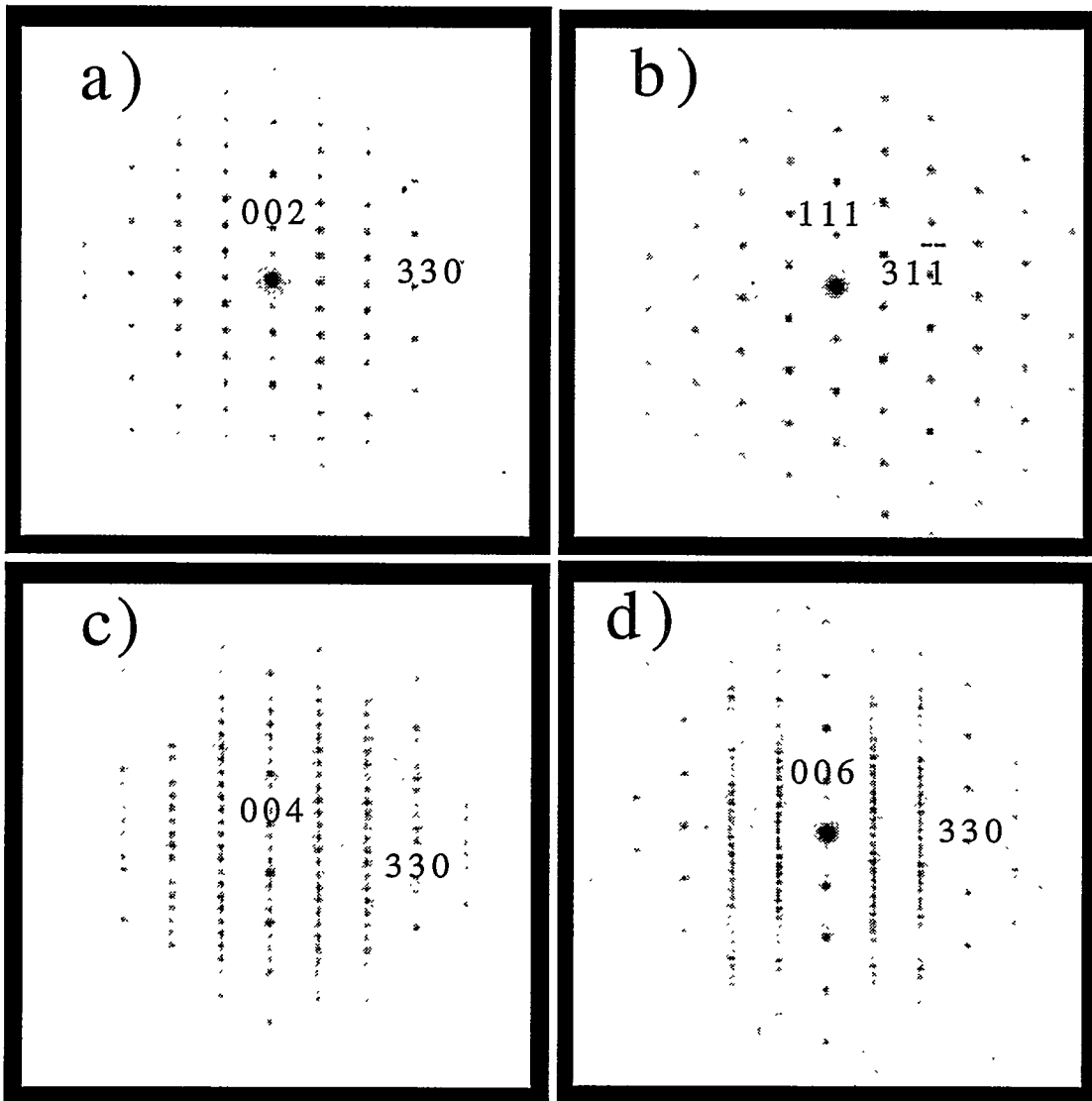


Figure 4. Selected area diffraction patterns from (a) C14, (b) C15, (c) C36 and (d) 6H, Laves polytypes, perpendicular to the primary stacking direction (vertical in figures). For hexagonal polytypes, this is the c-axis, which is equivalent to (111) in the case of C15.

## Discussion

### Microstructural Development

SEM characterization of the actinide-containing SS-15Zr alloys showed that the only observable change in the alloy microstructure for alloys with added actinides, compared to those without, was the presence of actinide-rich regions in the  $Zr(Fe,Cr,Ni)_{2+x}$  phase. The proportion of this phase increased with higher concentrations of added actinides. EDS analyses showed that the darkest contrast regions in the  $Zr(Fe,Cr,Ni)_{2+x}$  phase contained the least actinides and the brightest areas were the most enriched in actinides. No clear phase boundaries were observed between the actinide-rich areas and the actinide-deficient areas. The observed alloy microstructure appeared to be stable since no observable changes in alloy microstructure were detected in an actinide-containing alloy that had been heat-treated at 851°C for 100 hours (i.e., the actinides did not redistribute more evenly throughout the  $Zr(Fe,Cr,Ni)_{2+x}$  phase).

Table II. Intensity Ratios for Various Elements Observed in the Different Polytypes of the  $Zr(Fe,Cr,Ni)_{2+x}$  Phase.

Position	Structure	$I_U/I_{Zr}$	$I_{Fe}/I_{Cr}$	$I_{Fe}/I_{Ni}$	$I_N/I_{Cr}$
1	C15	0.461	11.42	2.98	3.82
2	C15	0.179	8.84	3.90	2.27
3	C15	0.312	9.08	3.65	2.49
4	C36	0.083	6.67	5.02	1.33
5	C36	0.107	7.85	4.56	1.77
6	C36	0.106	8.40	4.34	1.93
7	C36	0.108	8.04	4.35	1.85
8	C36	0.113	7.97	4.19	1.90
9	6H	0.120	7.66	4.57	1.67
10	6H	0.114	7.96	4.31	1.85
11	C14	0.037	6.22	5.44	1.14
12	C14	0.067	7.06	4.79	1.47
13	C14	0.035	6.10	5.82	1.05
14	C14	0.092	6.87	4.62	1.49

A central goal of the TEM investigation was to clarify the uneven distribution of Zr and U within the  $Fe_2Zr$  Laves compound phase, which was indicated by SEM, above. The approximately constant value of  $x_{Zr}+x_U \approx 0.24$  found using SEM semiquantitative X-EDS is an indication that the Zr and U can mix substitutionally on a single sublattice of the Laves compound structure. It is presumed that this is the A sublattice based on the metallic radii of U and Zr which are both approximately 1.58 Å, compared to the significantly smaller B components Cr, Fe and Ni (1.3 Å, 1.28 Å and 1.28 Å, respectively [9]). The presence of concentration gradients within a single alloy phase near to equilibrium is not expected from thermodynamics. A possible explanation for the observed gradients in the concentration of U/Zr is the existence of a number of Laves compound polytypes, which are frequently found simultaneously in a given alloy. These polytypes can be formed from each other by the insertion of ordered stacking defects, accomplished by migration of Shockley partial dislocations [8]. The TEM investigation was therefore undertaken in order to ascertain whether different tolerances for the substitution of U on Zr sites within various Laves compound polytypes, coupled with a locally varying structure, might explain the existence of the concentration gradients.

In addition to variations of the concentration of uranium, the data in Table 2 also suggest a systematic variation in the B-component concentrations ( $x_{Cr}$ ,  $x_{Fe}$ ,  $x_{Ni}$ ) depending on the Laves compound polytype. In particular, the C15 areas rich in uranium also tended to show more Fe and Ni relative to Cr, whereas the Zr-rich hexagonal C14 phase tended to show the most Cr and least Fe. The correlation of a B-component distribution with that of U is consistent with phase diagram information on the U and Zr-based binary systems. The uranium-chromium

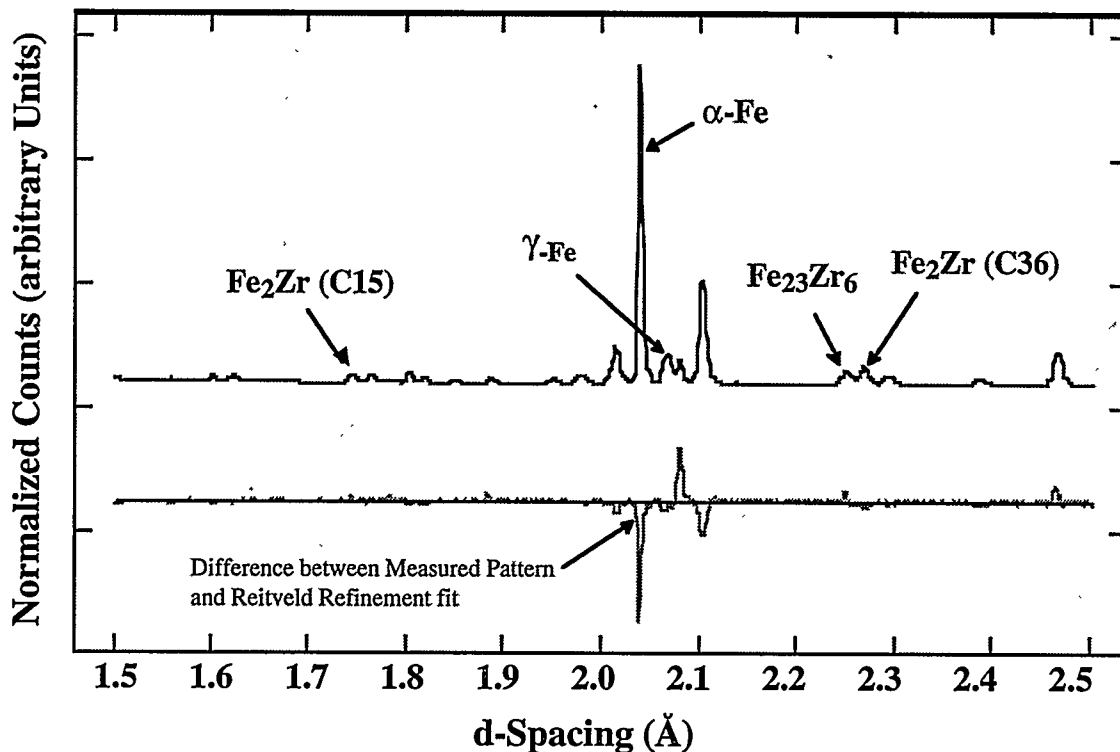


Figure 5. Neutron diffraction pattern from the SS-15Zr-5U alloy specimen. Uranium-rich phases are not observed; only phases typical of the SS-15Zr alloy are seen. A major peak from every phase has been identified.

Table III. Lattice Parameters (nm) and Volume Content (%) of Phases in SS-15Zr and SS-15Zr-5U alloy.

Phases	Lattice Parameters, nm			Phase Vol.%		
	Alloy Composition		% Change	Alloy Composition		Change
	SS-15Zr*	SS-15Zr-5U		SS-15Zr*	SS-15Zr-5U	
Ferrite	a=0.28760	a= 0.28759	-0.003	40 ± 6	45	+ 5
Austenite	a=0.35960	a= 0.35947	-0.036	9 ± 1	5	- 4
C36 Laves	a=0.49084	a= 0.49233	0.303	33 ± 5	13	- 20
	c=1.60162	c= 1.60164	0.001			
C15 Laves	a=0.69381	a= 0.69587	0.297	16 ± 2	21	+ 5
Fe <sub>23</sub> Zr <sub>6</sub> -type	a=1.16898	a= 1.16692	0.176	2 ± 1	17	+ 15

\*Data from REF. 5

system is immiscible [10], indicating small heats of mixing, whereas the ZrCr<sub>2</sub> C14 Laves compound is stable to 1673°C [11]. This can qualitatively explain the observation of Cr segregation to the Zr-rich hexagonal Laves compounds, as a result of thermodynamic or bonding characteristics. Thermodynamic assessments of the U-Ni and Zr-Ni binary systems indicate that both systems are characterized by strongly exothermic heats of formation [12,13], whereas the heat of formation of ZrFe<sub>2</sub> [14] appears to be somewhat more negative than for UFe<sub>2</sub> [15].

The high melting temperatures of  $ZrCr_2$  and  $ZrFe_2$  suggest that the initial composition of Laves compound crystals solidifying from the melt are rich in these elements, which may explain the tendency of U-rich regions to be located at the edge of Laves compound regions. On approaching equilibrium, a residual concentration gradient is retained, as it is stabilized by the existence of multiple polytypes within individual Laves compound regions. Under these circumstances, the B-component distribution may adjust corresponding to thermodynamic heat of mixing, which is consistent with uranium rich regions being low in Cr and high in Fe. The reason that a uranium and iron rich composition should stabilize C15, while Zr-rich regions higher in Cr prefer the C14 structure is a matter of speculation in the present case. The first neighbor coordinations are identical for all Laves compounds, so that an explanation on this level is not possible. In previous studies concerning other systems exhibiting multiple polytypes, it has frequently been found that polytype stability correlates with an electron per atom ( $e/a$ ) ratio [16,17], indicating the importance of electronic structure. A further possibility in the present case is that the more three-dimensional cubic C15 structure can tolerate a greater degree of disorder on the A-sites than the more planar hexagonal polytypes.

### Comparisons to SS-15Zr Alloy

The lattice parameters and volume content of phases in the SS-15Zr-5U alloy, as determined by neutron diffraction, are compared with those from an as-cast SS-15Zr alloy in Table 3. The lattice parameters of ferrite and austenite in the SS-15Zr-5U alloy are smaller than for the SS-15Zr alloy. Since uranium has a larger atomic radius than the major elements in ferrite and austenite, the smaller lattice parameters suggest the absence of uranium in these iron solid solution phases; this is in agreement with the results of SEM/EDS. Furthermore, since chromium addition is known to increase the lattice parameters of stainless steel phases [18], the smaller lattice parameters of ferrite and austenite in the SS-15Zr-5U alloy suggest a minor depletion of chromium from these phases.

The lattice parameters of the  $ZrFe_2$ -type Laves intermetallic phases, C36 and C15, are larger than the corresponding phases in the SS-15Zr alloy. In the C36 polytype, the "a" parameter shows an increase of 0.3%, whereas the "c" parameter only shows an increase of 0.001%. These results suggest an anisotropic distribution of uranium within the intermetallic; the uranium atom shows a strong preference for the basal planes of the hexagonal unit cell of the C36 intermetallic. The observed lattice expansions of the Laves intermetallics may be due to the substitution of uranium atoms at the Fe sites of the  $ZrFe_2$  lattice. Since the uranium atom is smaller than zirconium (but larger than iron) U substitution at Zr sites would have resulted in lattice contraction instead of the observed lattice expansions. Interestingly, the lattice parameters of the  $Fe_{23}Zr_6$ -type intermetallic are smaller in the uranium-containing alloy, suggesting U substitution at the Zr sites of this phase.

The volume content of phases in the SS-15Zr-5U and SS-15Zr alloys, calculated from the Reitveld refinements, is also shown in Table 3. The iron solid solution phase content in both SS-15Zr-5U and SS-15Zr alloys is ~50 vol%; there appears to be more ferrite but less austenite in the SS-15Zr-5U alloy. Significant differences are observed between the intermetallic phase contents of the SS-15Zr-5U and SS-15Zr alloys. The amounts of C15 and  $(Fe,Cr,Ni)_{23}Zr_6$  are larger and the amount of C36 is smaller in SS-15Zr-5U than in the SS-15Zr alloy. Preferential dissolution of U in C15 and  $(Fe,Cr,Ni)_{23}Zr_6$  may stabilize and increase the amount of these intermetallic phases. Since the U-rich regions of the  $Zr(Fe,Cr,Ni)_{2+x}$  phases exhibit enrichment in Ni, this may explain why the actinide-containing alloys show a reduction in the amount of austenite present. Less Ni is present to stabilize the austenite. Alternatively, minor variations in casting conditions (such as cooling rate effects) may account for the observed differences.

### **Conclusions**

Based on SEM, TEM, and neutron diffraction analyses of as-cast and heat-treated SS-15Zr alloys with added actinides, the following conclusions can be drawn:

1. As-cast SS-15Zr alloys with added actinides develop microstructures comprised of ferrite, austenite, the  $ZrFe_2$ -type Laves polytypes C14, C15, and C36, a  $Fe_{23}Zr_6$ -type intermetallic, and a phase with a 6-layer hexagonal structure. This microstructure is stable up to 850°C.
2. An uneven distribution of actinides within the  $Zr(Fe,Cr,Ni)_{2+x}$  phase is stabilized by different Laves phase polytypes (C14, C15, and C36) that are present. Each polytype contains different amounts of actinides.
3. Adding actinides to an SS-15Zr alloy results in an increase in the amounts of ferrite, Laves C15 and  $Fe_{23}Zr_6$ , and a decrease in the amounts of austenite and Laves C36. No new phases, not seen in SS-15Zr alloys without actinides, are observed.

### Acknowledgments

The U. S. Dept. of Energy, Office of Nuclear Energy, Science, and Technology, supported this work under contract W-31-109-Eng-38. Argonne National Laboratory is operated by the University of Chicago. Acknowledgment is given to R. Elliott, S. G. Johnson, and S. M. Frank for their assistance in the preparation of the alloys. Thanks is also given to M. C. Petri for conducting the heat treatment of the 3166SS-15Zr-10Pu alloy.

### References

1. W. Lutze, R. C. Ewing, Radioactive Waste Forms for the Future, North-Holland, Amsterdam, 1988.
2. J. J. Laidler, J. E. Battles, W. E. Miller, J. P. Ackerman, E. L. Carls, Prog. Nucl. Eng. 31 (1997) 131.
3. S. M. McDeavitt, D. P. Abraham, J. Y. Park, J. Nucl. Mater. 257 (1998) 21.
4. D. P. Abraham, S. M. McDeavitt, J. Y. Park, Metall. Mater. Trans. A 27A (1996) 2151.
5. D. P. Abraham, J. W. Richardson, Jr., S. M. McDeavitt, Mater. Sci. Engr. A239-240 (1997) 658.
6. C. W. Allen, P. Delavignette, S. Amelinckx, 9 (1972) 237.
7. D. B. Williams and C. B. Carter, Transmission Electron Microscopy Vol. II, Plenum Press, New York, 1996.
8. C. W. Allen and K. C. Liao, Phys. Stat. Sol. A 74 (1982) 673.
9. T. Egami and Y. Waseda, J. Non-Cryst. Sol. 64 (1984) 113.
10. L. R. Chapman and C. E. Holcombe, J. Nucl. Mater. 126 (1984) 323.
11. D. Arias and J. P. Abriata, Bull. Alloy Phase Diag. 7 (1986) 237.
12. P. Nash and C. S. Jayanth, in: P. Nash (Ed.) Phase Diagrams of Binary Nickel Alloys, ASM International, Materials Park, OH, 1991, p. 390.
13. D. E. Peterson, in: P. Nash (Ed.) Phase Diagrams of Binary Nickel Alloys, ASM International, Materials Park, OH, 1991, p. 358.
14. D. Arias, M. S. Granovsky, and J. P. Abriata, in: H. Okamoto (Ed.) Phase Diagrams of Binary Iron Alloys, ASM International, Materials Park, OH, 1993, p. 467.

15. H. Okamoto, in: T. B. Massalski (Ed.) Phase Diagrams of Binary Iron Alloys, Materials Park, OH, 1993, p. 429.
16. F. Laves and H. Witte, Metallwirtschaft 14 (1936) 840.
17. J. H. Zhu, P. K. Liaw, and C. T. Liu, Mater. Sci. Engr. A239-240 (1997) 260.
18. D. Peckner and I. M. Bernstein, Handbook of Stainless Steel, McGraw-Hill, New York, 1977.